Lasers in Manufacturing Conference 2019

Ultra-short pulse laser drilling: Requirements, constraints and strategies for upscaling.

David Brinkmeier[a,b*], Volkher Onuseit[b], Thomas Graf[a]

[a]*Institut für Strahlwerkzeuge (IFSW), University of Stuttgart, Pfaffenwaldring 43, 70569 Stuttgart, Germany*
[b]*Graduate School of advanced Manufacturing Engineering (GSaME), Nobelstrasse 12, 70569 Stuttgart, Germany*

Abstract

The availability of kW-class USP lasers leads to new challenges in order to scale laser drilling processes beyond their thermal limit. In this work, we discuss the implications and solutions to utilize next generation laser sources in drilling applications, based on an analytical heat accumulation model combined with an estimation of the achievable borehole geometry. Using this model it is possible to choose the right processing strategy, such as spatial parallelization and / or temporal sequencing, for an efficient use of kW-class USP lasers depending on laser parameters and the borehole geometry. Additionally the model allows the definition of selection criteria for an appropriate laser source, as well as focusing optics, for a desired borehole.

Keywords: Laser drilling; Heat accumulation; Drilling strategies; High average power ultrafast laser

1. Introduction

One of the major difficulties in material processing using ultra-short pulsed laser systems is finding a balance between quality constraints, for example in terms of roughness, melt expulsion or a heat affected zone and efficiency in terms of ablated volume per time and energy. The last consideration effectively requires the use of efficient processing parameters (Neuenschwander et al., 2012) and to fully utilize the available laser power. With the advent of kW-class ultra-short pulse (USP) laser sources heat accumulation presents a problem when trying to reconcile both considerations, especially in spatially concentrated

* Corresponding author. Tel.: +49 711 685 69747 .
E-mail address: david.brinkmeier@ifsw.uni-stuttgart.de .

processes such as drilling. Given the development of high-power USP laser sources, as presented in Fig. 1, strategies for upscaling the processes are required.

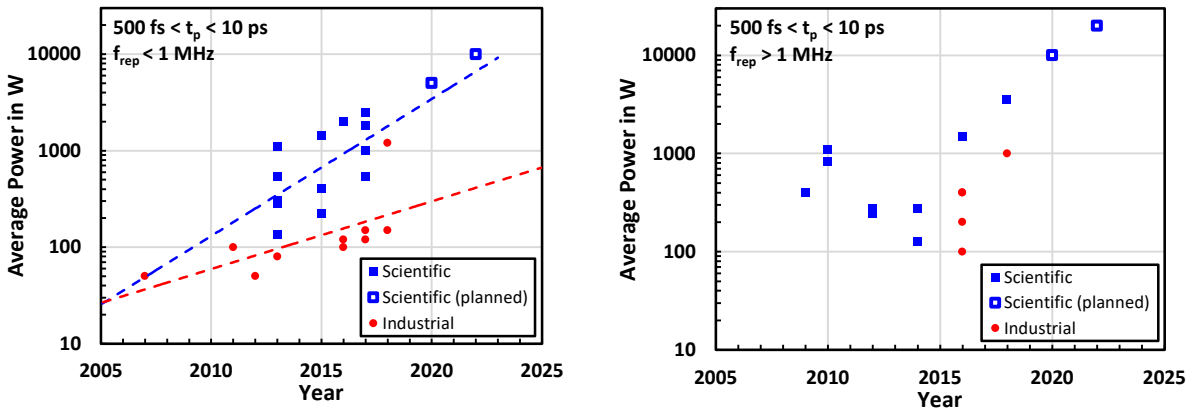

Fig. 1. (a) Development of scientific and industrial USP lasers with a pulse repetition rate below 1 MHz with exponential fits in dashed lines for scientific and industrial systems, (b) development of scientific and industrial USP lasers with a pulse repetition rate exceeding 1 MHz. Scientific results compiled from Brons et al., 2014; Hädrich et al., 2013; Klenke et al., 2013; Klingebiel et al., 2015; Mueller et al., 2017; Mueller et al., 2018; Negel, 2017; Negel et al., 2015; Negel et al., 2013; Nubbemeyer et al., 2017; Russbueldt et al., 2009; Russbueldt et al., 2010; Russbueldt et al., 2015; Saraceno et al., 2012; Saraceno et al., 2014; Sartorius et al., 2016; Schmidt et al., 2017; Teisset et al., 2017. Experimental (planned) from press release Fraunhofer ILT 04.07.2018 and industrial results from companies Active Fiber Systems, Amphos, Amplitude, Coherent, Edgewave and Trumpf.

To explore the constraints that arise in USP drilling, a semi-numerical heat accumulation model in conjunction with the achievable borehole geometry was used. In the case of the borehole geometry this relates primarily the borehole depth.

Using this simple model it is possible to pre-select an appropriate laser source for a given borehole and to derive the fundamental strategies which have to be employed when the thermal load prevents the use of the available laser power.

2. Modelling of USP-drilling processes

In order to derive conclusions and strategies for handling kW-class USP laser sources in drilling applications it is necessary to model the thermal constraints as well as the achievable borehole geometry and relate this information to possible laser sources. In order to verify our calculations and in order to model a realistic scenario, we adopt material parameters for the case of CrNi-steel processing.

For all following calculations, the material constants were taken from Weber et al., 2014 for the case of drilling in CrNi-steel and the threshold fluence is assumed to be 0.09 J/cm² in accordance with Förster et al., 2018. Both publications consider USP laser sources with pulse durations $t_p < 10$ ps at a wavelength of 1030 nm.

The residual heat η_{res} describes the part of the pulse energy E_P that contributes to heating the material, meaning

$$Q_{res} = E_p \cdot \eta_{res} \quad (1)$$

is the residual energy that contributes to heating the material. In the case of Weber et al., 2014 η_{res} is the result of a fit, whereas other sources (Bauer et al., 2015) measured this factor using calorimetry. The material properties for all following calculations are compiled in Table 1.

Table 1. Material properties, CrNi-steel

Property	Value	Unit
Thermal diffusivity κ	$0.4 \cdot 10^{-5}$	m²/s
Density ρ	7900	kg/m³
Heat capacity c_p	477	J/(kg·K)
Melting / Critical temperature T_{crit}	1500	°C
Residual heat η_{res}	0.125	
Threshold fluence φ_{th}	0.09	J/cm²

2.1. Heat accumulation

We consider the case of 3D heat conduction, where the incident pulse is modeled as a delta function in time and as a Gaussian surface with variance w_0 in the plane of absorption (focal plane) spatially. Bauer et al., 2015 present an analytic solution for a Gaussian heat source of this type. The solution of the temperature field is given as

$$T^{s.p.}_{(r_c,z_c)}(r,z,t) = T_0 + \frac{2Q_{res}}{\pi\rho c_p\sqrt{\pi\kappa t}\cdot(8\kappa t + w_0^2)} \cdot e^{-\frac{(r-r_0)^2+(z-z_0)^2}{4\kappa t}\left(\frac{w_0^2}{8\kappa t+w_0^2}-1\right)} \cdot e^{-\frac{z^2}{4\kappa t}} \quad (2)$$

after a single incident pulse which is offset by the environment temperature T_0. The term $(r\text{-}r_0)$ and $(z\text{-}z_0)$ respectively denote the distances from the center of the Gaussian distribution. For the solution at the center of the beam as well as its focal plane $(r = r_0 = 0,\ z = z_0 = 0)$ equation (2) simplifies to

$$T^{s.p.}_{(r_c,z_c)}(r,z,t) = T_0 + \frac{2Q_{res}}{\pi\rho c_p\sqrt{\pi\kappa t}\cdot(8\kappa t+w_0^2)}. \quad (3)$$

Like Weber et al., 2014 and Bauer et al., 2015 it is assumed that the temperature increase evaluated at the origin caused by heat accumulation after N_p pulses is the relevant parameter regarding processing quality. Furthermore, it is assumed that the critical temperature threshold is the melting temperature of the material and that the material parameters are constant with respect to the temperature, which allows for linear superposition of subsequent pulses. These assumptions are in line with the considerations of Weber et al., 2014 for the case of USP drilling and have been experimentally validated in the aforementioned paper. The temperature increase resulting from the N-th pulse impinging on the surface with a repetition rate f_{rep} evaluated at time t is then given by

$$\Delta T(0,t) = \frac{2Q_{res} \cdot \Theta\left(t - \frac{N-1}{f_{rep}}\right)}{\pi^{\frac{3}{2}} \rho c_p \sqrt{\kappa}} \cdot \frac{1}{8\kappa\left(t - \frac{N-1}{f_{rep}}\right)^{\frac{3}{2}} + w_0^2\left(t - \frac{N-1}{f_{rep}}\right)^{\frac{1}{2}}} \quad (4)$$

after rearranging. Θ denotes the Heaviside function and the temperature is calculated at a time delay of $((N-1)/f_{rep})$ after the first pulse hits the target at time $t = 0$. Evaluating this sum after the N_p-th pulse, i.e. $t = N_p/f_{rep}$, yields

$$\Delta T_{sum}\left(0, \frac{N_p}{f_{rep}}\right) = \frac{2Q_{res}}{\pi^{\frac{3}{2}} \rho c_p \sqrt{\kappa}} \cdot \sum_{N=1}^{N_p} \frac{1}{\frac{8\kappa}{f_{rep}{}^{\frac{3}{2}}} \cdot N^{\frac{3}{2}} + \frac{w_0^2}{f_{rep}{}^{\frac{1}{2}}} \cdot N^{\frac{1}{2}}}, \quad (5)$$

in which case Θ from equation (4) evaluates to one for every pulse and the sum in equation (5) is similar to the harmonic series (p-series). As can be seen, equation (5) contains scaling factors dependent on κ, f_{rep} and w_0 inside the sum for $w_0 \neq 0$. In the case of an ideal point source ($w_0 = 0$) equation (5) simplifies to

$$\Delta T_{sum}\left(0, \frac{N_p}{f_{rep}}\right) = \frac{2Q_{res}}{\rho c_p \left(\frac{4\pi\kappa}{f_{rep}}\right)^{\frac{3}{2}}} \cdot \sum_{N=1}^{N_p} \frac{1}{N^{\frac{3}{2}}}. \quad (6)$$

The expression in equation (6) is in line with the derivation from the ideal point source as presented in Weber et al., 2014. The sum in equation (6) is the well-known harmonic series (p-series) with $p = 1.5$, which is known to converge for $p > 1$. Thus, the sum converges and evaluates to

$$\sum_{N=1}^{\infty} \frac{1}{N^{\frac{3}{2}}} = \zeta\left(\frac{3}{2}\right) \approx 2.612375.. \quad (7)$$

where ζ is the Riemann zeta function. The sum in equation (5) can be shown to converge in a rigorous manner as well, but convergence is easily understood when considering that a sum of convergent series is itself convergent and acknowledge the fact that the solution for the Gaussian heat source is derived from a sum (integral) of point sources over a Gaussian surface (Bauer et al., 2015). In addition, in Weber et al., 2017 an explicit approximate analytical expression for the temporal evolution of the sum as a function of the number of incident pulses N for $w_0 = 0$ is derived. Due to the lack of an analytical approximation to the sum in the case of the Gaussian heat source, the sum was calculated numerically. In Fig. 2 (a) and (b) respectively the evaluation of the heat accumulation for a single set of laser parameters in the case of the point source and a Gaussian heat source is shown.

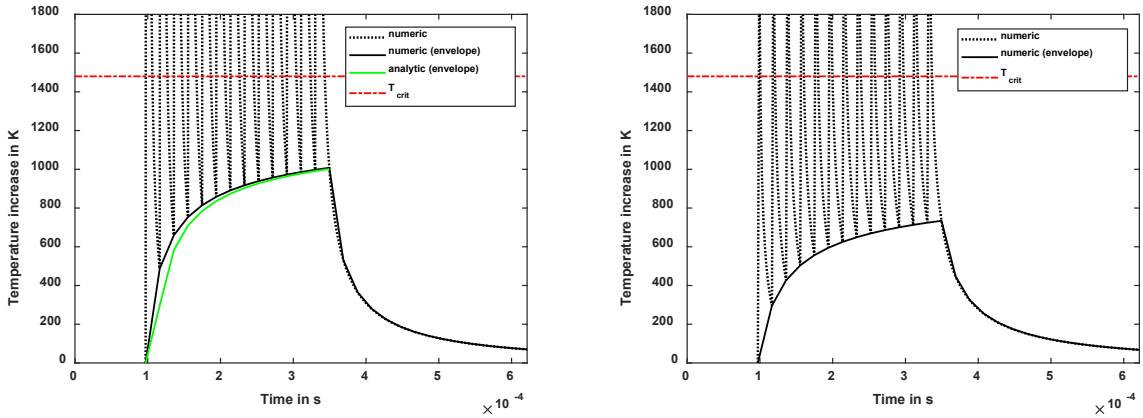

Fig. 2. (a) Temporal evolution of the temperature increase on the surface of a semi-infinite body of CrNi-steel at the location of a point source and (b) in the case of a Gaussian heat source with a beam diameter of d_0 = 40 µm. Parameters for the calculation are a repetition rate of f_{rep} 51.5 kHz and a pulse energy of E_p = 200 µJ. In the case of the point source the analytic approximation presented in Weber et al., 2017 is additionally plotted, which shows a slight deviation from the numerical result for the first heat inputs, as reported. The temperature increase in the case of a Gaussian heat source is noticeably lower, as expected.

2.2. Borehole geometry

In regards to the borehole geometry the model given by Förster et al., 2018 was adopted, where the achievable depth in the case of high quality percussion drilled holes, i.e. when thermal damage and excessive melting is avoided, is derived as

$$z_{drill,limit} = w_0 \cdot \sqrt{\frac{4\phi_{avg}^2 - \phi_{th}^2 \cdot \ln\left(\frac{2\phi_{avg}}{\phi_{th}}\right)^2}{2\phi_{th}^2 \cdot ln\left(\frac{2\phi_{avg}}{\phi_{th}}\right)}} \tag{8}$$

with the average fluence $\phi_{avg} = E_p/(\pi w_0^2)$ and the entrance diameter

$$r_{abl,entrance} = w_0 \cdot \sqrt{\frac{1}{2} \cdot \ln\left(\frac{2\phi_{avg}}{\phi_{th}}\right)} \tag{9}$$

for a Gaussian beam. Furthermore, in Förster et al., 2018 it is assumed that the process is terminated before an irregular drilling process sets in. This “irregular drilling” sets in when the drilling rate significantly decreases towards reaching the depth limit of the drilling process. This event is accompanied by the formation of multiple borehole tails in random directions at the bottom of the borehole, as shown in Döring et al., 2010. Thus, the depth per equation (8) is not to be taken as the maximum achievable depth, but the depth that one should not try to exceed for reproducible holes of high quality: Holes of conical shape without significant thermal damage or melt generation. To denote these qualities and avoid confusion with

what is commonly thought of when speaking of a borehole depth, we will call this depth quality depth limit for the remainder of this paper.

3. Results

We combine the heat accumulation and quality depth limit in a single graph by calculating the critical number of pulses $N_{p,crit}$ until reaching T_{crit}, evaluated over the range **Ep** and $\mathbf{f_{rep}}$ at a constant w_0. Since laser sources which fulfill the condition

$$P_{avg}(E_p, f_{rep}) = E_p \cdot f_{rep} = const. \qquad (10)$$

appear as straight lines in a log-log graph, they can be conveniently superimposed with the critical number of pulses as displayed in Fig. 3. For simplicity, in Fig. 3 the critical number of pulses is resolved only in three distinct areas:

1. *Green:* $N_{p,crit} = \infty$: An infinite number of pulses can be deposited without reaching T_{crit}.
2. Yellow: $\infty > N_{p,crit} > 1$: A finite number of pulses can be deposited without reaching T_{crit}.
3. *Red:* $N_{p,crit} = 1$: only a single pulse can be deposited upon which a subsequent pulse would hit the target at a temperature above T_{crit}.

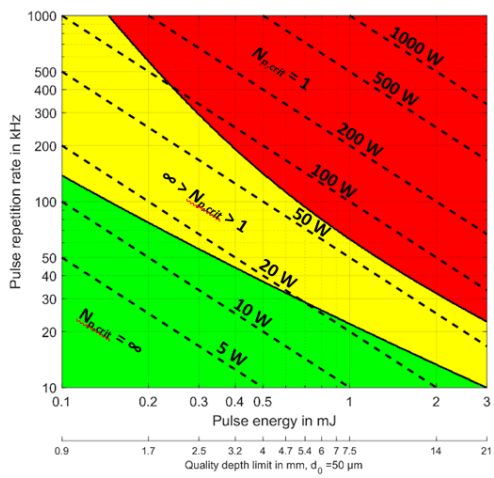

Fig. 3. Evaluation of the heat accumulation for w_0 = 25 µm over a large range of pulse repetition rates and pulse energies. The color coding represents the critical number of pulses divided into the relevant three areas. The dashed lines represent all possible laser sources for a given average power and the secondary horizontal axis displays the fluence-dependent depth limit given in equation (8).

In the first case the average laser power can be used permanently, in the second case waiting periods have to be introduced periodically and in the third case processing is not viable for drilling one hole.

Now consider as an example drilling a 4 mm deep hole with an entrance diameter of 85 µm ≤ d_{abl} ≤ 100 µm using a beam diameter (in focus) of 50 µm and a laser source with an average power of 200 W at a pulse energy of E_p = 1 mJ and pulse repetition rate f_{rep} = 200 kHz. Then, according to equation (9) the upper limit in terms of the pulse energy is 3 mJ due to the constraints regarding d_{abl}, while the lower limit to reach a depth of 4 mm is 500 µJ according to equation (9). As can be seen in Fig. 3, the parameters E_p = 1 mJ and f_{rep} = 200

kHz would put the process well into the red zone. Thus, in order to avoid heat accumulation f_{rep} and / or E_p have to be reduced, while continuing the use of the available full average power. The only way to do this is to implement parallelization or sequencing,

$$
\begin{aligned}
P_{avg} = const. = \; & n_{holes} \cdot E_p \cdot \frac{f_{rep}}{i}, && n_{holes} = [1,2,3 \dots], i = n_{holes} && \text{sequencing} \\
\triangleq \; & n_{holes} \cdot \frac{E_p}{k} \cdot f_{rep}, && n_{holes} = [1,2,3 \dots], k = n_{holes} && \text{parallelization} \qquad (11) \\
\triangleq \; & n_{holes} \cdot \frac{E_p}{i} \cdot \frac{f_{rep}}{k}, && n_{holes} = [1,2,3 \dots], ik = n_{holes} && \text{combination}
\end{aligned}
$$

As can be seen in equation (11), any attempt at resolving the issue results in drilling more than one borehole at a time, i.e. we can reduce the effective repetition rate per hole by an integer number using a scanning system (sequencing) or use a beam splitter (parallelization), in which case the effective pulse energy is reduced. In both cases, the output repetition rate and pulse energy of the laser source is required to be constant in order to maintain the full average power output.

In the case of sequencing this requires a fast and accurate beam deflection system that is able to move the beam between holes on a timescale of f_{rep}^{-1} s. In the case of sequencing the effective pulse repetition rate per hole can only be reduced using integer dividers, e.g. going from one drilling at 200 kHz to two drillings at 100 kHz. In the case of parallelization an ideal beam splitter without power losses and identical beam profiles is desirable. Such a setup would reduce the effective pulse energy per hole. In principle beam splitters other than those which distribute the energy equally could be used, but this would result in varying drilling processes, borehole geometries and processing times. Hence, for each drilling an identical pulse energy should be applied. As a consequence, this variant also requires division into an integer number of boreholes using beam splitters of equal energy distribution.

The application of the discussed strategies is visualized in Fig. 4, where the laser source is marked as a red polygon at E_p = 1 mJ and f_{rep} = 200 kHz. In this graph, moving horizontally to the left from the starting point towards lower effective average powers implies the use of parallelization. Alternatively, sequencing implies a reduction of the effective repetition rate, meaning vertical movement downwards in the graph.

Applying the constraints for the mentioned example it is clear that a reduction of the effective pulse energy below 500 µJ is not permitted, which means that through parallelization alone it is impossible to realize this process at an average laser power of 200 W. In contrary, through sequencing, or a combination of parallelization and sequencing, processing is possible.

In this example an appropriate processing strategy was derived for a given laser source and borehole. Alternatively, one can instead choose an appropriate laser source for a given borehole or specify parameters for the design of a laser source due to the thermal and geometric requirements of a specific borehole and processing strategy (parallelization / sequencing). However, using only these selection criteria one should not expect to select an ideal laser source. As explained in the introduction, in that case the efficiency of the process needs to be taken into account as well.

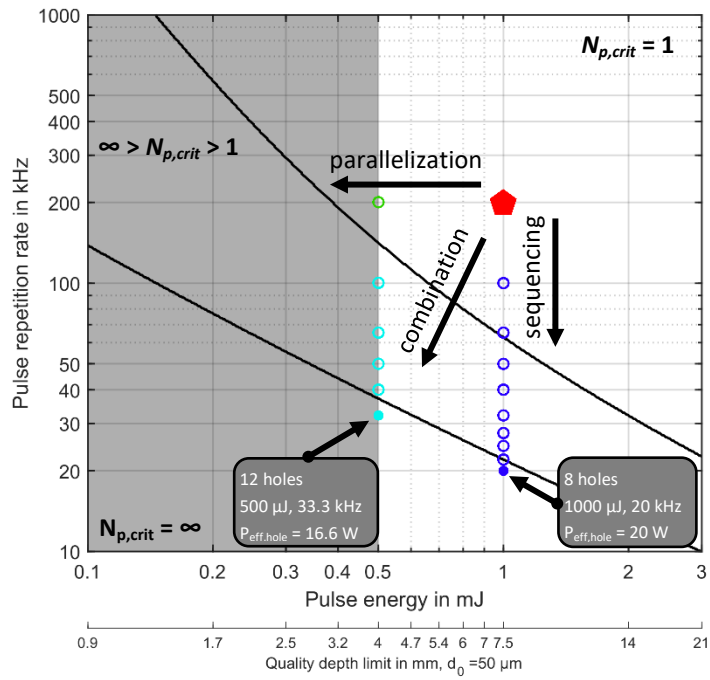

Fig. 4. (a) Application of the strategies parallelization and sequencing starting from the non-viable processing point indicated by the red polygon representing the laser source operating at its maximum average power output. For the case of a 4 mm deep drilling at w_0 = 25 µm, the constraints regarding pulse energy ($0.5\ \mathrm{mJ} \leq E_p \leq 3\ \mathrm{mJ}$) and heat accumulation result in the possible processing parameters as indicated in the figure.

It should be noted that both concepts (parallelization / sequencing) have already been discussed and implemented to varying degrees in literature. The last statement is true primarily for the case of parallelization, i.e. whenever parallel processing is realized through a reduction of the effective pulse energy: Examples of these are methods based on diffractive elements (Haupt et al., 2011, Pulsar Photonics GmbH), dynamic diffractive elements (Kuang et al., 2009, Kuang et al., 2014) as well as combinations using refractive elements (Salter and Booth, 2011). The case of sequencing is discussed as a possibility in Loor et al., 2014 where the application of a polygon scanner based system is considered to deliver a “percussion-like process by multipass operation”. As noted by Loor et al., one of the primary concerns in such a process is the positioning error of the scanning system.

4. Conclusion

In this paper we presented a way to combine and visualize laser drilling processes over a large range of parameters in order to derive processing constraints for high power USP drilling. Fundamentally, the only solution to implement USP laser drilling processes using next generation laser sources requires drilling of several boreholes at the same time. This can be achieved through a parallelization, sequencing or combination of both strategies. Given that high pulse energies are a necessity for deep drilling of holes and that the heat accumulation scales linearly with the energy input but disproportionately with the pulse repetition rate, in many cases sequencing is required. Further research will deal with the implications and considerations for optical systems in order to realize these strategies for helical drilling applications.

References

Neuenschwander, Beat; Jaeggi, Beat; Schmid, Marc; Rouffiange, Vincent; Martin, Paul-E. (2012): Optimization of the volume ablation rate for metals at different laser pulse-durations from ps to fs. In: Guido Hennig, Xianfan Xu, Bo Gu und Yoshiki Nakata (Hg.): Laser Applications in Microelectronic and Optoelectronic Manufacturing (LAMOM) XVII. SPIE LASE. San Francisco, California, USA, Saturday 21 January 2012: SPIE (SPIE Proceedings), S. 824307.

Brons, Jonathan; Pervak, Vladimir; Fedulova, Elena; Bauer, Dominik; Sutter, Dirk; Kalashnikov, Vladimir et al. (2014): Energy scaling of Kerr-lens mode-locked thin-disk oscillators. In: *Optics letters* 39 (22), S. 6442–6445. DOI: 10.1364/OL.39.006442.

Hädrich, Steffen; Klenke, Arno; Hoffmann, Armin; Eidam, Tino; Gottschall, Thomas; Rothhardt, Jan et al. (2013): Nonlinear compression to sub-30-fs, 0.5 mJ pulses at 135 W of average power. In: *Optics letters* 38 (19), S. 3866–3869. DOI: 10.1364/OL.38.003866.

Klenke, Arno; Breitkopf, Sven; Kienel, Marco; Gottschall, Thomas; Eidam, Tino; Hädrich, Steffen et al. (2013): 530 W, 1.3 mJ, four-channel coherently combined femtosecond fiber chirped-pulse amplification system. In: *Optics letters* 38 (13), S. 2283–2285. DOI: 10.1364/OL.38.002283.

Klingebiel, Sandro; Schultze, Marcel; Teisset, Catherine Y.; Bessing, Robert; Häfner, Matthias; Prinz, Stephan et al. (2015): 220mJ Ultrafast Thin-Disk Regenerative Amplifier. In: 2015 Conference on Lasers and Electro-Optics (CLEO). 10 - 15 May 2015, San Jose, CA. CLEO: Science and Innovations. San Jose, California. Optical Society of America; Conference on Lasers and Electro-Optics; CLEO. Piscataway, NJ: IEEE, STu4O.2.

Mueller, M.; Klenke, A.; Stark, H.; Buldt, J.; Gottschall, T.; Limpert, J.; Tünnermann, A. (2017): 16 Channel Coherently-Combined Ultrafast Fiber Laser. In: Laser Applications Conference. Part of Laser Congress : 1-5 October 2017, Nagoya, Aichi, Japan. Advanced Solid State Lasers. Nagoya, Aichi. Optical Society of America; LAC; Laser Congress; OSA Laser Congress. Washington, D.C., USA: OSA - The Optical Society (OSA technical digest (online)), AW4A.3.

Mueller, Michael; Klenke, Arno; Steinkopff, Albrecht; Stark, Henning; Tünnermann, Andreas; Limpert, Jens (2018): 3.5 kW coherently combined ultrafast fiber laser. In: *Optics letters* 43 (24), S. 6037–6040. DOI: 10.1364/OL.43.006037.

Negel, Jan-Philipp (2017): Scheibenlaser-Multipassverstärker für ultrakurze Laserpulse mit Ausgangsleistungen im kW-Bereich. Dissertation. Herbert Utz Verlag GmbH; Universität Stuttgart.

Negel, Jan-Philipp; Loescher, André; Voss, Andreas; Bauer, Dominik; Sutter, Dirk; Killi, Alexander et al. (2015): Ultrafast thin-disk multipass laser amplifier delivering 1.4 kW (4.7 mJ, 1030 nm) average power converted to 820 W at 515 nm and 234 W at 343 nm. In: *Optics express* 23 (16), S. 21064–21077. DOI: 10.1364/OE.23.021064.

Negel, Jan-Philipp; Voss, Andreas; Abdou Ahmed, Marwan; Bauer, Dominik; Sutter, Dirk; Killi, Alexander; Graf, Thomas (2013): 1.1 kW average output power from a thin-disk multipass amplifier for ultrashort laser pulses. In: *Optics letters* 38 (24), S. 5442–5445. DOI: 10.1364/OL.38.005442.

Nubbemeyer, Thomas; Kaumanns, Martin; Ueffing, Moritz; Gorjan, Martin; Alismail, Ayman; Fattahi, Hanieh et al. (2017): 1 kW, 200 mJ picosecond thin-disk laser system. In: *Optics letters* 42 (7), S. 1381–1384. DOI: 10.1364/OL.42.001381.

Russbueldt, P.; Mans, T.; Rotarius, G.; Weitenberg, J.; Hoffmann, H. D.; Poprawe, R. (2009): 400W Yb:YAG Innoslab fs-Amplifier. In: *Opt. Express* 17 (15), S. 12230. DOI: 10.1364/OE.17.012230.

Russbueldt, P.; Mans, T.; Weitenberg, J.; Hoffmann, H. D.; Poprawe, R. (2010): Compact diode-pumped 1.1 kW Yb:YAG Innoslab femtosecond amplifier. In: *Optics letters* 35 (24), S. 4169–4171. DOI: 10.1364/OL.35.004169.

Russbueldt, Peter; Hoffmann, Dieter; Hofer, Marco; Lohring, Jens; Luttmann, Jorg; Meissner, Ansgar et al. (2015): Innoslab Amplifiers. In: *IEEE J. Select. Topics Quantum Electron.* 21 (1), S. 447–463. DOI: 10.1109/JSTQE.2014.2333234.

Saraceno, Clara J.; Emaury, Florian; Heckl, Oliver H.; Baer, Cyrill R. E.; Hoffmann, Martin; Schriber, Cinia et al. (2012): 275 W average output power from a femtosecond thin disk oscillator operated in a vacuum environment. In: *Optics express* 20 (21), S. 23535–23541. DOI: 10.1364/OE.20.023535.

Saraceno, Clara J.; Emaury, Florian; Schriber, Cinia; Hoffmann, Martin; Golling, Matthias; Südmeyer, Thomas; Keller, Ursula (2014): Ultrafast thin-disk laser with 80 µJ pulse energy and 242 W of average power. In: *Optics letters* 39 (1), S. 9–12. DOI: 10.1364/OL.39.000009.

Sartorius, T.; Russbueldt, P.; Bauer, P.; Sutter, D.; Hoffmann, D. (2016): Innoslab and thin-disk amplifier system with 1.5 kW average power at 710 fs pulse duration. In: Solid State Lasers XXV: Technology and Devices. Lase. San Francisco. SPIE, S. 9726–9742.

Schmidt, Bruno E.; Hage, Arvid; Mans, Torsten; Légaré, François; Wörner, Hans Jakob (2017): Highly stable, 54mJ Yb-InnoSlab laser platform at 0.5kW average power. In: *Optics express* 25 (15), S. 17549–17555. DOI: 10.1364/OE.25.017549.

Teisset, Catherine Yuriko; Schultze, Marcel; Bessing, Robert; Häfner, Matthias; Prinz, Stephan; Sutter, Dirk; Metzger, Thomas (2017): 300 W Picosecond Thin-Disk Regenerative Amplifier at 10 kHz Repetition Rate. In: Laser Applications Conference. Part of Laser Congress : 1-5 October 2017, Nagoya, Aichi, Japan. Advanced Solid State Lasers. Nagoya, Aichi. Optical Society of America; LAC; Laser Congress; OSA Laser Congress. Washington, D.C., USA: OSA - The Optical Society (OSA technical digest (online)), JTh5A.1.

Fraunhofer ILT (04.07.2018): Fraunhofer entwickelt neue Lasergeneration. Hoffmann, Hans Dieter; Limpert, Jens. online available at https://www.ilt.fraunhofer.de/de/presse/pressemitteilungen/pm2018/pressemitteilung-2018-7-4.html, last checked on 28.04.2019.

Weber, Rudolf; Graf, Thomas; Berger, Peter; Onuseit, Volkher; Wiedenmann, Margit; Freitag, Christian; Feuer, Anne (2014): Heat accumulation during pulsed laser materials processing. In: *Optics express* 22 (9), S. 11312–11324. DOI: 10.1364/OE.22.011312.

Förster, Daniel J.; Weber, Rudolf; Holder, Daniel; Graf, Thomas (2018): Estimation of the depth limit for percussion drilling with picosecond laser pulses. In: *Optics express* 26 (9), S. 11546–11552. DOI: 10.1364/OE.26.011546.

Bauer, Franziska; Michalowski, Andreas; Kiedrowski, Thomas; Nolte, Stefan (2015): Heat accumulation in ultra-short pulsed scanning laser ablation of metals. In: *Optics express* 23 (2), S. 1035–1043. DOI: 10.1364/OE.23.001035.

Weber, Rudolf; Graf, Thomas; Freitag, Christian; Feuer, Anne; Kononenko, Taras; Konov, Vitaly I. (2017): Processing constraints resulting from heat accumulation during pulsed and repetitive laser materials processing. In: *Optics express* 25 (4), S. 3966–3979. DOI: 10.1364/OE.25.003966.

Döring, Sven; Richter, Sören; Nolte, Stefan; Tünnermann, Andreas (2010): In situ imaging of hole shape evolution in ultrashort pulse laser drilling. In: *Optics express* 18 (19), S. 20395–20400. DOI: 10.1364/OE.18.020395.

Haupt, Oliver; Schütz, Viktor; Stute, Uwe (2011): Multi-spot laser processing of crystalline solar cells. In: Laser-based Micro- and Nanopackaging and Assembly V. SPIE LASE. San Francisco, California, USA, Saturday 22 January 2011: SPIE (SPIE Proceedings), 79210V.

Pulsar Photonics GmbH: Multibeam Scanner MBS. online available at https://www.pulsar-photonics.de/systemtechnik/multibeam-scanner-mbs/, last checked on 06.05.2019.

Kuang, Zheng; Perrie, Walter; Liu, Dun; Edwardson, Stuart; Cheng, Jian; Dearden, Geoff; Watkins, Ken (2009): Diffractive multi-beam surface micro-processing using 10ps laser pulses. In: *Applied Surface Science* 255 (22), S. 9040–9044. DOI: 10.1016/j.apsusc.2009.06.089.

Kuang, Zheng; Perrie, Walter; Edwardson, Stuart P.; Fearon, Eamonn; Dearden, Geoff (2014): Ultrafast laser parallel microdrilling using multiple annular beams generated by a spatial light modulator. In: *J. Phys. D: Appl. Phys.* 47 (11), S. 115501. DOI: 10.1088/0022-3727/47/11/115501.

Salter, Patrick S.; Booth, Martin J. (2011): Addressable microlens array for parallel laser microfabrication. In: *Optics letters* 36 (12), S. 2302–2304. DOI: 10.1364/OL.36.002302.

Loor, Ronny de; Penning, Lars; Slagle, Rick (2014): Polygon Laser Scanning. In: *LTJ* 11 (3), S. 32–34. DOI: 10.1002/latj.201400033.